Accuracy of a hybrid finite-element method for solving a scattering Schrödinger equation

Joseph Power and George Rawitscher
Physics Department, University of Connecticut, Storrs, Connecticut 06269, USA
(Received 20 August 2012; revised manuscript received 25 September 2012; published 21 December 2012)

This hybrid method [finite-element discrete variable representation (FE-DVR)], introduced by Resigno and McCurdy [Phys. Rev. A **62**, 032706 (2000)], uses Lagrange polynomials in each partition, rather than "hat" functions or Gaussian functions. These polynomials are discrete variable representation functions, and they are orthogonal under the Gauss-Lobatto quadrature discretization approximation. Accuracy analyses of this method are performed for the case of a one-dimensional Schrödinger equation with various types of local and nonlocal potentials for scattering boundary conditions. The accuracy is ascertained by a comparison with a spectral Chebyshev integral equation method, accurate to $1:10^{-11}$. For an accuracy of the phase shift of $1:10^{-8}$, the FE-DVR method is found to be 100 times faster than a sixth-order finite-difference method (Numerov), it is easy to program, and it can routinely achieve an accuracy of better than $1:10^{-8}$ for the numerical examples studied.

DOI: 10.1103/PhysRevE.86.066707 PACS number(s): 02.60.Gf, 02.70.−c, 34.50.−s

I. INTRODUCTION

The solution of differential equations by means of expansions into discrete variable representation (DVR) basis functions has become very popular since it was first introduced in the early 1960s [1]. A review can be found in the paper by Light and Carrington [2], and generalizations to multidimensional expansions are also under development [3].

Previously, the main application of the DVR method was for obtaining bound-state energies and wave functions. For this purpose, the wave function is expanded into a set of N basis functions, whose expansion coefficients are to be determined. The calculations are of the Galerkin type, namely, the Hamiltonian applied to the wave function is multiplied on the left by each one of the expansion basis functions, and the result is integrated over the full range of the domain of the variable, leading to a set of N linear equations for the expansion coefficients. The integrals to be evaluated are then approximated by discrete sums over the values of the integrand evaluated at the support points times certain weight factors such as in the Gauss quadrature methods [4].

In the case of the solution of scattering problems, the finite-element method (FEM) [5] has also been developed. In this procedure, the radial range is divided into partitions, also called elements, and the solution of the wave equation in each partition is expanded into basis functions such as "hat" functions, Gaussians, or polynomials of a given order, whose expansion coefficients are to be determined. The equations for the expansion coefficients are obtained through a Galerkin procedure, and in many cases the integrals over the basis functions can be done analytically. The continuity of the wave function from one partition to the next is achieved by imposing conditions on the expansion coefficients, as is done, for example, in Ref. [6]. In the more recent DVR methods, the basis functions are Lagrange polynomials whose zeros occur at the Lobatto points [7,8], in which case the quadrature is denoted as Gauss-Lobatto, and the basis set of functions is denoted as Lagrange-Lobatto. This basis set was first suggested by Manolopoulos and Wyatt [9], and an extensive review is given in Ref. [10]. The main computational advantage of using DVR basis functions is that the sum mentioned above reduces to only one term, because the product of two different DVR functions vanishes at the support points, and only products between the same DVR functions remain. Furthermore, within the approximation of the Gauss-Lobatto quadrature rule, the basis functions are orthogonal. Hence the procedure leads to a discretized Hamiltonian ($N \times N$) matrix, whose eigenfunctions determine the expansion coefficients and the eigenvalues determine the bound-state energies. There are several types of errors introduced by this method. One is due to the truncation of the expansion of the wave function in terms of basis functions at an upper limit N. Another is due to the approximation of the Gauss-Lobatto quadrature described above in terms of discrete sums over the support points. A third error is the accumulation of machine round-off errors. These errors have been examined for bound-state energy eigenvalues [3,11–13], and it is found that the convergence of the energy with the number N of DVR basis functions is exponential, and the nonorthogonality error becomes small as N increases.

Very recently, a combination of the FE and DVR methods was introduced into atomic physics by Rescigno and McCurdy [14] for quantum scattering calculations. These calculations use the FEM approach, but in each partition the basis functions are Lagrange polynomials, and the support points are Gauss-Lobatto. This "hybrid" method, denoted as FE-DVR, is now used extensively for atomic physics calculations, such as for multielectron density distributions in atoms [15], for photoionizing cross sections with fast photon pulses [16,17], and for atom-atom scattering calculations [18], to name a few. However, in these works the accuracy of the results was not studied in detail. The FE-DVR method has also been used extensively for fluid dynamic calculations since the 1980s [19] and is also used in seismology [20], where it is called the spectral element method.

The main purpose of the present study is to investigate the accuracy of the FE-DVR method for the scattering conditions, since all the errors described above (the Gauss-Lobatto integration error, the truncation errors of the expansions, and the accumulation of round-off errors) are still present. In our study, a method of imposing the continuity of the wave function and of the derivative from one partition to the next is explicitly given, and the accuracy is obtained by comparing the

results of the FE-DVR calculation for particular solutions of a one-dimensional Schrödinger equation with a spectral [21] Chebyshev expansion method [22], S-IEM. The accuracy of the latter is of the order of $1:10^{-11}$, as is demonstrated in Appendix A. In our present formulation of the FE-DVR, the so-called bridge functions used in Refs. [14–18] in order to assure the continuity of the wave function are not used, but they are replaced by our present method.

In Sec. II, the FE-DVR method is described, in Sec. III, the accuracy is investigated by means of numerical examples, and Sec. IV contains the summary and conclusions. Appendix A contains a short review of the S-IEM method, in Appendix B an estimate of the accumulation of errors is presented, and in Appendix C a comparison with the finite difference Numerov (or Milne's) method is presented.

II. THE FE-DVR METHOD

The FE-DVR version of the finite-element method differs from the conventional FEM in that the basis functions for the expansion of the solution $\psi(x)$ in each partition are N "discrete variable representation" functions, which in the present case are Lagrange polynomials $\ell_i(x)$, $i = 1,2,\ldots,N$, of a given order $N-1$,

$$\ell_i(x) = \prod_{k=1}^{N} \frac{(x-x_k)}{(x_i-x_k)}, k \neq i \tag{1}$$

defined, for example, in Eq. (25.2.2) of Ref. [23], and in section 3.3(i) of Ref. [4]. These functions are widely used for interpolation procedures and are described in standard computational textbooks. This FE and DVR combination was introduced in Ref. [14], and it has the advantage that integrals involving these polynomials amount to sums over the functions evaluated only at the support points. In the present case, the support points are Lobatto points x_j and weights w_j, $j = 1,2,\ldots,N$, defined in Eq. (25.4.32) of Ref. [23], in terms of which a quadrature over a function $f(x)$ in the interval $[-1,+1]$ is approximated by

$$\int_{-1}^{+1} f(x)\,dx \simeq \sum_{j=1}^{N} f(x_j) w_j. \tag{2}$$

If f is a polynomial of degree $\leqslant 2N-3$, then Eq. (2) will be exact. This, however, is not the case for the product of two Lagrange polynomials $\ell_i(x)\ell_j(x)$, a polynomial of order $2(N-1)$. In the Gauss-Lobatto quadrature approximation [7,8], given by the right-hand side of Eq. (2), these Lagrange polynomials are orthogonal to each other, but they are not rigorously orthogonal [12] because the left-hand side of Eq. (2) is not equal to the right-hand side. If the integral limits are different from ± 1, such as $\int_a^b f(r)dr$, then the variable r can be scaled to the variable x. Our method differs from that of Ref. [14] in that we do not use their "bridge" functions, but rather ensure continuity of the solution and its derivative from one partition to the next by using only the Lagrange functions. Since the Lobatto points are not evenly spaced, expansion (2) converges uniformly, which is a general feature of spectral methods [21]. A further DVR advantage is that the Gauss-Lobato approximation of the integral

$$\int_{-1}^{1} \ell_i(x) f(x) \ell_j(x) dx \simeq \delta_{i,j} w_j f(x_i) \tag{3}$$

is diagonal in i,j and is given by only one term. The convolution

$$\int_{-1}^{1} \ell_i(x) \int_{-1}^{1} K(x,x') \ell_j(x') dx'\, dx \simeq w_i w_j K(x_i,x_j) \tag{4}$$

is also approximated by one nondiagonal term only, which is a marked advantage for solving nonlocal or coupled channel Schrödinger equations. The kinetic energy integral can be expressed in the form

$$\int_{-1}^{1} \ell_i(x) \frac{d^2}{dx^2} \ell_j(x) dx = -\int_{-1}^{1} \ell_i'(x)\ell_j'(x)dx + \delta_{i,N}\ell_j'(1) - \delta_{i,1}\ell_j'(-1) \tag{5}$$

after an integration by parts. In the above, the prime denotes d/dx. The integral on the right-hand side of this equation can be done exactly with the Gauss-Lobatto quadrature rule (2), since the integrand is a polynomial of order $2N-4$, which is less than the required $2N-3$.

For the case of a local potential V with angular momentum number $L = 0$, the equation to be solved is

$$\left(\frac{d^2}{dr^2} + k^2\right)\psi(r) = V(r)\psi(r), \tag{6}$$

and for a nonlocal potential K, the term $V(r)\psi(r)$ is replaced by $\int_0^\infty K(r,r')\psi(r')dr'$. The wave number k is in units of fm^{-1} and the potential V is in units of fm^{-2}, where quantities in energy units are transformed to inverse length units by multiplication by the well known factor $2m/\hbar^2$. In the scattering case, the solutions $\psi(r)$ are normalized such that for $r \to \infty$ they approach

$$\psi(r) \to \sin(kr) + \tan(\delta)\cos(kr), \tag{7}$$

and with that normalization one finds

$$\tan(\delta) = -\frac{1}{k}\int_0^\infty \sin(kr) V(r)\psi(r) dr, \tag{8}$$

as is well known [24].

The FE-DVR procedure is as follows. We divide the radial interval into N_J partitions (also called elements in the finite-element calculations [5]), and in each partition we expand the wave function into N Lagrange functions $\ell_i(r)$, $i = 1,2,\ldots,N$,

$$\psi^{(J)}(r) = \sum_{i=1}^{N} c_i^{(J)} \ell_i(r), \quad b_1^{(J)} \leqslant r \leqslant b_2^{(J)}. \tag{9}$$

The starting and end points of each partition are denoted as $b_1^{(J)}$ and $b_2^{(J)}$, respectively. We define the value and the derivative of the wave function at the end point of the previous partition as

$$\psi^{(J-1)}\left(b_2^{(J-1)}\right) = c_N^{(J-1)}, \tag{10}$$

where $c_N^{(J-1)}$ is the last coefficient of the expansion (9) of $\psi^{(J-1)}$, and

$$A^{(J-1)} \equiv \frac{d}{dr}\psi^{(J-1)}\left(b_2^{(J-1)}\right) = \sum_{i=1}^{N} c_i^{(J-1)} \ell\,'_i\left(b_2^{(J-1)}\right), \quad (11)$$

respectively, where $\ell\,'_i(r) = d\ell_i(r)/dr$. The result (10) follows from the fact that $\ell_i(b_2) = 0$ for $i = 1,2,\ldots,N-1$, and $\ell_N(b_2) = 1$. For the first partition, we arbitrarily take a guessed value of $A^{(0)}$ for the nonexisting previous partition, and later we renormalize the whole wave function by comparing it to a known value. That is equivalent to renormalizing the value of $A^{(0)}$. In finite-element calculations, continuity conditions of the wave function from one partition to the next are also imposed. However, the method described below applies specifically to the case in which the basis functions in each element are of the DVR type, rather than general polynomials of a given order [6].

By performing the Galerkin integrals of the Schrödinger equation over the ℓ_i in each partition J,

$$\langle \ell_i(T + V - k^2)\psi^{(J)}\rangle = \int_{b_1^{(J)}}^{b_2^{(J)}} \ell_i(r)(T + V - k^2)\psi^{(J)}(r)dr = 0,\ i = 1,2,\ldots,N, \quad (12)$$

we obtain a homogeneous matrix equation in each partition for the coefficients $c_i^{(J)}$, $i = 1,2,\ldots,N$,

$$M^{(J)}\,\vec{c}^{(J)} = 0, \quad (13)$$

where $\vec{c}^{(J)}$ represents the $(N \times 1)$ column vector of the coefficients $c_i^{(J)}$, and where the matrix elements of M are given by $M_{ij} = \langle \ell_i(T + V - k^2)\ell_j\rangle$. Here $T = -d^2/dr^2$. The continuity conditions are imposed by transforming the homogeneous equation (13) of dimension N into an inhomogeneous equation of dimension $N-2$ whose driving terms are composed of the function ψ and $d\psi/dr$ evaluated at the end of the previous partition. These conditions are given by

$$c_1^{(J)} = c_N^{(J-1)}, \quad (14)$$

where use has been made of $\ell_i(b_1) = 0$ for $i = 2,\ldots,N$, and $\ell_1(b_1) = 1$, and

$$\frac{d\psi^{(J-1)}\left(b_2^{(J-1)}\right)}{dr} = \sum_{i=1}^{N} c_i^{(J)} \ell\,'_i\left(b_1^{(J)}\right) = A^{(J-1)}. \quad (15)$$

These two conditions can be written in the matrix form

$$F_{11}\alpha + F_{12}\beta = \gamma, \quad (16)$$

where

$$F_{11} = \begin{pmatrix} 1 & 0 \\ \ell'_1 & \ell'_2 \end{pmatrix}^{(J)}_{b_1^{(J)}}, \quad F_{12} = \begin{pmatrix} 0 & 0 & \cdots & 0 \\ \ell'_3 & \ell'_4 & \cdots & \ell'_N \end{pmatrix}^{(J)}_{b_1^{(J)}}, \quad (17)$$

where

$$\alpha = \begin{pmatrix} c_1 \\ c_2 \end{pmatrix}^{(J)}, \quad (18)$$

where

$$\beta = \begin{pmatrix} c_3 \\ c_4 \\ \vdots \\ c_N \end{pmatrix}^{(J)}, \quad (19)$$

and where

$$\gamma = \begin{pmatrix} c_N \\ A \end{pmatrix}^{(J-1)}. \quad (20)$$

With that notation, Eq. (13) can be written in the form

$$\begin{pmatrix} M_{11} & M_{12} \\ M_{21} & M_{22} \end{pmatrix}\begin{pmatrix} \alpha \\ \beta \end{pmatrix} = 0, \quad (21)$$

where the matrix $M^{(J)}$ has been decomposed into four submatrices M_{11}, M_{12}, M_{21}, and M_{22}, which are of dimension $2 \times 2, 2 \times (N-2), (N-2) \times 2$, and $(N-2) \times (N-2)$, respectively. The column vector α can be eliminated in terms of β and γ by using Eq. (16),

$$\alpha = F_{11}^{-1}(-F_{12}\beta + \gamma), \quad (22)$$

and the result when introduced into Eq. (21) leads to an inhomogeneous equation for β,

$$\left(-M_{21}F_{11}^{-1}F_{12} + M_{22}\right)\beta = -M_{21}F_{11}^{-1}\gamma. \quad (23)$$

Once the vector β is found from Eq. (23), then the components of the vector α can be found from Eq. (22), and the calculation can proceed to the next partition.

If one expresses the inverse of F_{11} analytically,

$$F_{11}^{-1} = \begin{pmatrix} 1 & 0 \\ -\frac{\ell'_1}{\ell'_2} & \frac{1}{\ell'_2} \end{pmatrix}, \quad (24)$$

then one finds

$$F_{11}^{-1}\gamma = \begin{pmatrix} c_N^{(J-1)} \\ -\frac{\ell'_1}{\ell'_2}c_N^{(J-1)} + \frac{A^{(J-1)}}{\ell'_2} \end{pmatrix} \quad (25)$$

and

$$F_{11}^{-1}F_{12} = \begin{pmatrix} 0 & 0 & \cdots & 0 \\ \frac{\ell'_3}{\ell'_2} & \frac{\ell'_4}{\ell'_2} & \cdots & \frac{\ell'_N}{\ell'_2} \end{pmatrix}. \quad (26)$$

Inserting (24) into Eq. (22), one finds that $c_1^{(J)} = c_N^{(J-1)}$, but $c_2^{(J)}$ is a function of $c_N^{(J-1)}$, $A^{(J-1)}$, and the vector β.

III. ACCURACY

We have tested the accuracy for cases with angular momentum $L = 0$ for two local potentials V_M and $V_{\rm WS}$, shown in Fig. 1, and for a nonlocal potential $K(r,r')$ of the Perey-Buck type [25]. Potential V_M is of a Morse type with a repulsive core near the origin, given by

$$V_M(r) = 6\exp(-0.3\,r + 1.2)[\exp(-0.3\,r + 1.2) - 2], \quad (27)$$

and $V_{\rm WS}$ is a short-ranged simple Woods-Saxon potential given by

$$V_{\rm WS}(r) = -3.36/\{1 + \exp[(r - 3.5)/0.6]\}. \quad (28)$$

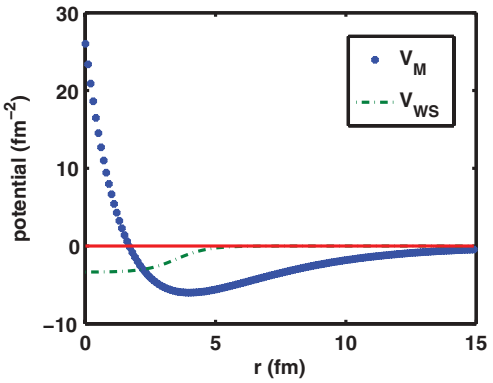

FIG. 1. (Color online) Morse (V_M) and Woods-Saxon ($V_{\rm WS}$) potentials as a function of radial distance r. These potentials are given by Eqs. (27) and (28), respectively.

The coefficients 6 and -3.36 are in units of fm^{-2}, the distances r are in units of fm, and all other factors are such that the arguments of the exponents are dimensionless. These potentials are shown in Fig. 1, and the respective wave functions are shown in Fig. 2. The choice of these potentials is motivated by the difference in the degree of computational difficulty that they offer in the solution of the Schrödinger equation. The potential $V_{\rm WS}$ has no repulsive core near the origin and is of short range. Hence the corresponding wave function does not have large derivatives near the origin, and it need not be calculated out to distances larger than 20 fm, where the potential is already negligible, of the order of 10^{-11}. In contrast, neither of these two features applies for the case of V_M. To obtain an accuracy of $1:10^{-11}$, the wave function has to be calculated out to 100 fm, as is indeed done in the calculation of the benchmark S-IEM solution, and the repulsive core near the origin is more difficult to treat. The nonlocal potential K is described in Eq. (3) of Ref. [26] together with the Appendix of Ref. [25]. The accuracy of the corresponding wave function obtained with the S-IEM method for this nonlocal potential is illustrated in Fig. 7 of Ref. [26]. For the nonlocal case, only one partition is used in the FE-DVR method, which extends from $r=0$ to $R_{\rm max}$, but in view of Eq. (4), the calculation is very efficient.

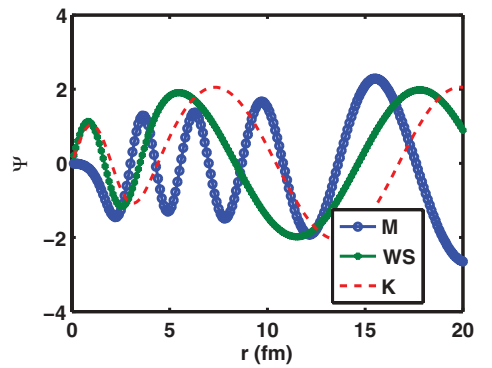

FIG. 2. (Color online) The wave functions for the local potentials V_M and $V_{\rm WS}$, and for the nonlocal potential K, described in the text. The wave number is $k=0.5$ fm^{-1} and the potentials V_M and $V_{\rm WS}$ are illustrated in Fig. 1.

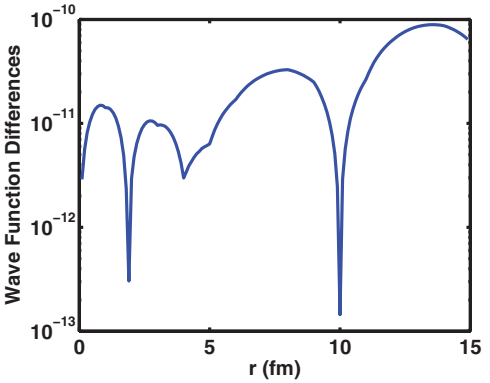

FIG. 3. (Color online) Accuracy of the FE-DVR solution of the Schrödinger equation for the Woods-Saxon potential $V_{\rm WS}$ displayed in Fig. 1. The wave number is $k=0.5$ fm^{-1}, the size of each partition is 1 fm, and there are 20 Lobatto points per partition. The graph shows the accuracy of the wave function ψ by displaying the absolute value of the difference between the FE-DVR and the S-IEM wave functions. The latter is deemed accurate to $1:10^{-11}$.

To ascertain the accuracy of the FE-DVR method, the solutions of Eq. (6) are compared with the solutions obtained by the spectral integral equation method (S-IEM) [22], whose accuracy is $1:10^{-11}$, as described in Appendix A. The numerical FE-DVR solutions are first normalized by a comparison with the S-IEM solutions at one chosen radial position near the origin, and the error of the normalized FE-DVR function is determined by a comparison with the S-IEM function at all other radial points r. Since the S-IEM function depends on the values of the potential at all points $[0\leqslant r\leqslant R_{\rm max}]$, the S-IEM calculation has to be carried out to a distance $R_{\rm max}$ large enough so that the contribution from $V(r\geqslant R_{\rm max})$ is smaller than the desired accuracy of the S-IEM solution. The same is not the case for the FE-DVR solutions $\psi_{\rm FE-DVR}(r)$, since the unnormalized solution depends only on the potentials for distances less than r. However, if the normalization of the wave function (7) is to be accomplished by matching it to $\sin(kr)$ and $\cos(kr)$ at $R_{\rm max}$ in the asymptotic region, then the numerical errors that accumulated out to $R_{\rm max}$ will affect the

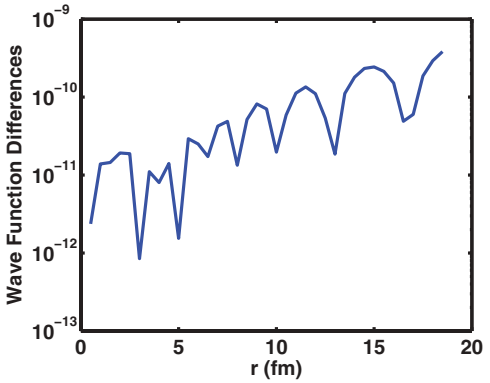

FIG. 4. (Color online) The accuracy of the FE-DVR wave function for the potential V_M as obtained by comparison with the S-IEM result. The latter is accurate to $1:10^{-11}$. The wave number is $k=0.5$ fm^{-1}, the number of Lobatto points per partition is 20, and the size of each partition is 1 fm.

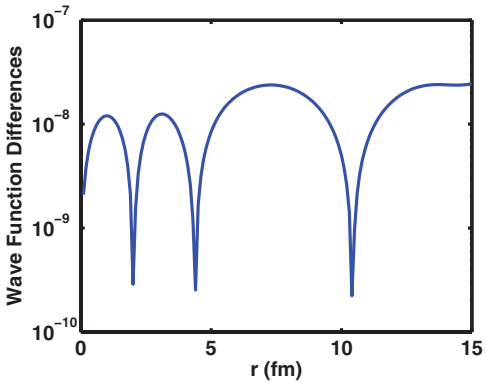

FIG. 5. (Color online) Same as Fig. 3 for the nonlocal Perey-Buck potential $K(r,r')$. The wave number is $k = 0.5$ fm^{-1}; only one partition was used in the full radial interval from 0 to 15 fm using a total of 130 Lobatto grid points. The accuracy of 10^{-8} is consistent with the estimate made in Eq. (B4) in Appendix B.

wave function at all distances. These errors can be avoided by an iterative procedure for the large distance part of the wave function, as will be described in a future publication [27].

The results for potentials $V_{\rm WS}$ and V_M are shown Figs. 3 and 4, respectively. In both cases, the error of the wave function starts with 10^{-11} at small distances, and it increases to 10^{-10} as the distance increases, due to the accumulation of various errors. The accuracy for the nonlocal potential K is shown in Fig. 5. The accuracy of the integral (8), for a fixed size of all partitions as a function of the number N of Lobatto points in each partition, is shown in Fig. 6, where the open circles represent an upper limit of the estimated accuracy as developed in Appendix B, of order $(N-2)^3$. This figure is important because it shows the nearly exponential increase of accuracy as N increases, until the accumulation of errors overwhelms this effect once the value of N increases beyond

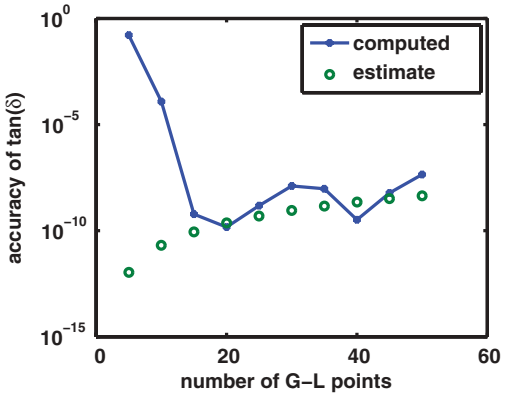

FIG. 6. (Color online) Accuracy of the integral $\int_0^{100} \sin(kr)\ V_M(r)\ \psi(r)\ dr$, obtained with the FE-DVR method as a function of the number of Lobatto points in each partition. The length of each partition is 1.0 fm and the number of partitions is 100. The potential is V_M, the wave number is $k = 0.5$ fm^{-1}, and the accuracy is obtained by comparison with the S-IEM result, which is accurate to $1 : 10^{-11}$. The open circles represent an estimate of the upper bound for the accumulation of roundoff errors, given by Eq. (B1) in Appendix B.

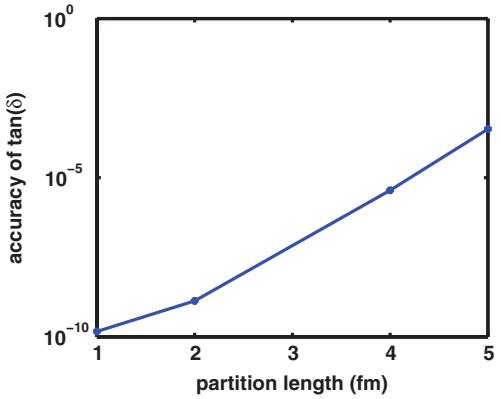

FIG. 7. (Color online) Accuracy of the integral $\int_0^{100} \sin(kr)\ V_M(r)\ \psi(r)\ dr$, Eq. (8), as a function of the length of each partition, into which the radial interval [0,100 fm] is divided. The total number $N = 20$ of Lobatto points in each partition is kept constant. The conditions are the same as in Fig. 6. This figure shows that the accuracy decreases exponentially with the size of the partition. For 20 partitions, the computation time is 0.060 s; for 100 partitions, it is 0.075 s.

a certain value, 20 for the case of Fig. 6. The accuracy of the integral (8) for a fixed number N per partition, but for several different partition sizes, is displayed in Fig. 7. This figure shows that the accuracy decreases exponentially with the size of the partition, which can be interpreted as an exponential increase of the accuracy with the number of Lobatto points in each partition of fixed length.

Finally, the FE-DVR computing time as a function of the number N of Lobatto points in each partition is displayed in Fig. 8, where it is also compared with an estimate described in Appendix B of the number of floating point operations expected. According to this estimate, the time per floating point operation turns out to be $\simeq 10^{-8}$ in a MATLAB computation performed on a desktop using an Intel TM2 Quad, with a CPU Q 9950, a frequency of 2.83 GHz, and a RAM of 8 GB. The dashed line represents the total time required for a comparable S-IEM computation. That comparison shows that the FE-DVR method can be substantially faster than S-IEM even though the former has many more support points, depending on the radial range and on the accuracy required. Further details are given in Table II in Appendix A.

A comparison between the FE-DVR and a finite-difference sixth-order Numerov method of the accuracy of $\tan(\delta)$ is illustrated in Fig. 9.

This comparison shows that for an accuracy of $\tan(\delta)$ of $\simeq 10^{-8}$, the FE-DVR method requires 15 times fewer mesh

TABLE I. Accuracy and computing time for the S-IEM method.

Tol.	Part′ (ns)	Points	Error [tan(δ)]	Time (s)
10^{-12}	37	629		0.178
10^{-10}	25	425	4.6×10^{-12}	0.181
10^{-8}	17	289	7.7×10^{-11}	0.171
10^{-6}	11	187	5.2×10^{-7}	0.165
10^{-4}	7	119	2.8×10^{-4}	0.162
10^{-2}	5	85	6.5×10^{-2}	0.161

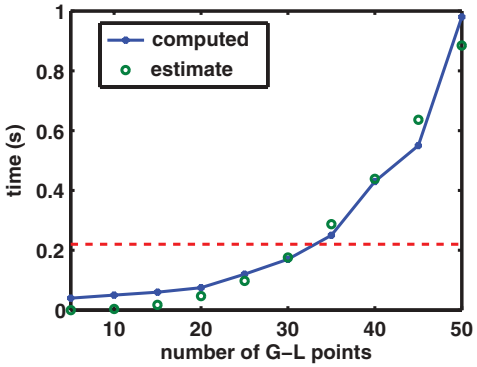

FIG. 8. (Color online) The computing time in MATLAB for the calculations described in Fig. 6. The estimate is given by Eq. (B1), with the factor 10^{-16} replaced by 2×10^{-8}. The latter represents the time for each floating point operation. The dashed line represents the computing time for the S-IEM calculation, described in Fig. 6.

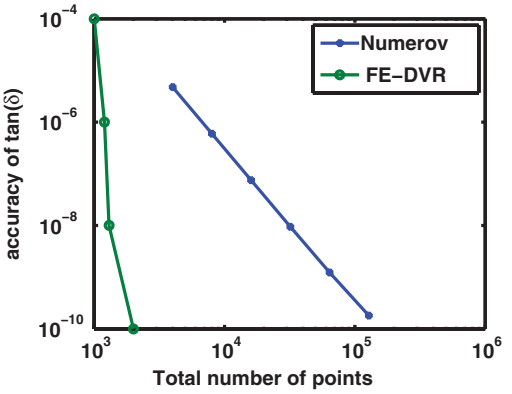

FIG. 9. (Color online) This accuracy comparison for $\tan(\delta)$ is performed for the potential V_M and $k = 0.5\ \mathrm{fm}^{-1}$ in the radial interval [0,100 fm]. The partition sizes in the FE-DVR method have a length of 1 fm each, and the number of Lobatto points in each partition is given by 1/100th of the total number of points. Numerov is a sixth-order finite-difference method with equidistant points, as described in Appendix C.

points, and is approximately 100 times faster than the Numerov method. More details are presented in Appendix C.

IV. SUMMARY AND CONCLUSIONS

The accuracy of a hybrid finite-element method (FE-DVR) has been examined for the solution of the one-dimensional Schrödinger equation with scattering boundary conditions. This method [14] uses as basis functions the discrete variable representation Lagrange polynomials $\ell_i(r)$, $i = 1,2,\ldots,N$, on a mesh of N Lobatto support points. The accuracy of the FE-DVR method is obtained by comparison with a spectral method S-IEM, whose accuracy is of the order of $1 : 10^{-11}$. An important advantage of a discrete variable representation basis is the ease and accuracy with which integrals can be performed using a Gauss-Lobatto integration algorithm that furthermore renders the matrix elements $\langle \ell_i(V-E)\ell_j \rangle$ diagonal. This feature permits one to easily solve the Schrödinger equation also in the presence of nonlocal potentials with a kernel of the form $K(r,r')$, as is demonstrated in one of our numerical examples. Another advantage is that the Galerkin matrix elements of the kinetic energy operator T need not be recalculated anew for each partition because they are the same in all partitions to within a normalization factor that only depends on the size of the partition. A further advantage is that the convergence of the expansion (9) with the number N of basis functions is exponential, in agreement with what is the case for bound-state finite-element calculations with Lobatto discretizations [12]. A possible disadvantage may be that if the number of the Lagrange polynomials in each partition is very large and/or the number of partitions is large, as is the case for long-ranged potentials, then the accumulation of roundoff and algorithm errors may become unacceptably large.

TABLE II. Accuracy and computing time for the FEM-DVR method.

No. of points	Error [$\tan(\delta)$]	Time (s)
2000	10^{-10}	0.075
1300	10^{-8}	0.050
1200	10^{-6}	0.047
1000	10^{-4}	0.045
700	10^{-2}	0.042

In summary, for scattering solutions of the Schrödinger equation, the accuracy of the FE-DVR method increases exponentially with the number of Lagrange polynomials in each partition until the accumulation of roundoff and truncation errors overwhelms the result. The FE-DVR can easily achieve an accuracy of the order of 10^{-10} for the scattering phase shifts for either local or nonlocal short-ranged potentials; it is less complex than the spectral S-IEM method, but it is comparable with regard to the amount of computing time; and, in addition, it is substantially more efficient than a finite-difference Numerov method. The latter result is demonstrated by the fact that the FE-DVR was found to be 100 times faster than the Numerov method for an accuracy of 10^{-8} of the scattering phase shift.

ACKNOWLEDGMENTS

One of the authors (G.R.) is grateful to C. W. McCurdy for a stimulating conversation on the use of Lagrange polynomials in finite-element calculations.

APPENDIX A: THE S-IEM METHOD

A version of the spectral method employed here was developed recently [22]. It consists in dividing the radial interval into partitions of variable size, and obtaining two independent solutions of the Schrödinger Eq. (6) in each partition, denoted as $Y(x)$ and $Z(x)$. These solutions are obtained by transforming Eq. (6) into an equivalent Lippmann-Schwinger integral equation (LS) and solving the latter by expanding the solution into Chebyshev functions, mapped to the interval $[-1,+1]$. The corresponding discretized matrices are not sparse, but are of small dimension equal to the number of Chebyshev points per partition. The solution ψ in each partition is obtained by a linear combination of the two

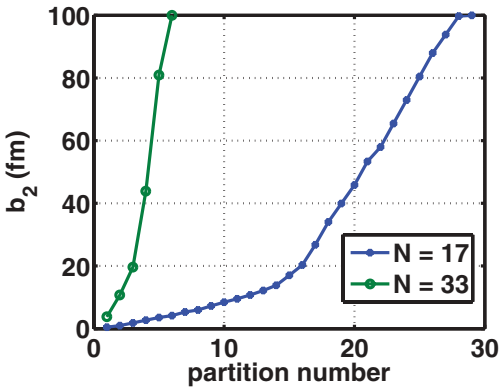

FIG. 10. (Color online) The partition distribution for the S-IEM method in the radial interval [0,100 fm] for two different numbers N of the Chebyshev expansion functions in each partition. The end point b_2 of each partition is shown on the vertical axis, and the corresponding partition number is shown on the horizontal axis. The potential is V_M, and the wave number is $k = 0.5$ fm^{-1}. The accuracy parameter "tol." in each partition is 10^{-12}. The computation time for each case is approximately the same, 0.2 s, and the accuracy of the wave function in both cases is the same, $1 : 10^{-11}$.

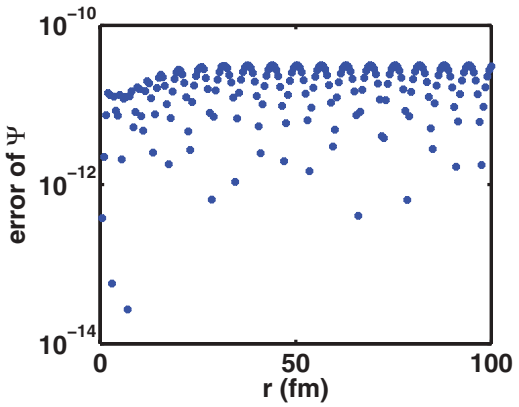

FIG. 11. (Color online) The y axis illustrates the absolute value of the difference between two S-IEM wave functions, calculated with accuracy parameters tol. $= 10^{-11}$ and 10^{-12}, respectively, for potential V_M and $k = 0.5$ fm^{-1}. This difference is less than 4×10^{-11} for all values of r.

independent functions $Y(x)$ and $Z(x)$, with coefficients that are determined from the solution of a matrix equation of dimension twice as large as the number of partitions, but the corresponding matrix is sparse. Details are given in Ref. [22], and a pedagogical version is found in Ref. [28].

One of the features of the S-IEM method is that the size of each partition is adaptively determined such that the accuracy of the functions $Y(x)$ and $Z(x)$ is equal to or better than a predetermined accuracy parameter tol., which in the present case is tol. $= 10^{-12}$. In the region where the potential V is small, the corresponding partition size is large. When the number of Chebyshev expansion functions N per partition is large, the size of the partitions is correspondingly large. As is illustrated in Fig. 10, when N is increases from 17 to 33, the number of partitions decreases from 29 to 6, yet the accuracy of the respective wave functions is approximately the same, $1 : 10^{-11}$, and the computing time is also approximately the same, 0.2 s.

For the present S-IEM benchmark calculations, the value of N is 17, and for the case of V_M the maximum value of r is 100 fm. Such a large value is required because the potential decays slowly with distance and becomes less in magnitude than 5×10^{-12} only beyond $r = 100$ fm. Had the potential been truncated at a smaller value of r, then the truncation error would have propagated into all values of the wave function and rendered it less accurate. The accuracy of the S-IEM wave function can be seen from Fig. 11, which compares two S-IEM wave functions with accuracy parameters tol. $= 10^{-11}$ and 10^{-12}, respectively. The result is that the accuracy of the IEM wave function for $N = 17$ and $R_{\max} = 100$ fm and tol. $= 10^{-11}$ is 4×10^{-11}, and that for tol. $= 10^{-12}$ the accuracy is better than 10^{-11}.

The wave functions are normalized such that their asymptotic value is given by Eq. (7). The corresponding values of $\tan(\delta)$, Eq. (8), for potentials V_M and $V_{\rm WS}$ and a wave number $k = 0.5$ fm^{-1} are 2.699 470 250 2 and $-1.710\,734\,422\,7$, respectively. Table I shows the number of partitions, the accuracy of $\tan(\delta)$, and the computing time of the S-IEM method for various tolerance parameters input into the code for the potential V_M, with $k = 0.5$. The number of Chebyshev polynomials in each partition is 17; the total number of points displayed in the third column is equal to 17 times the number of partitions. The error of $\tan(\delta)$ is obtained by comparing the value of $\tan(\delta)$ for a particular tolerance parameter with the value obtained for tol. $= 10^{-12}$.

For the case of a nonlocal potential K, the division of the radial interval into partitions is not made because the effect of the nonlocal potential would extend into more than one partition, making the programming more cumbersome. For the case of a kernel $K(r,r')$, described in Ref. [26], the accuracy of the S-IEM result [26] is also good to $1 : 10^{-11}$, as is shown in Fig. 7 of Ref. [26].

For comparison with the S-IEM method, some characteristics of the FE-DVR method are shown in Table II. The potential and the wave number are the same as in Table I, the radial interval [0,100 fm] is divided into 100 partitions of length 1 fm each, and the number of Lobatto points per partition in all partitions is the same but is progressively varied from 20 to 7, as shown in the table. If one compares the entries in Table I with those in Table II that correspond to approximately the same accuracy of 10^8 for $\tan(\delta)$, one notices that the FE-DVR method needs approximately seven times more support points than the S-IEM does, yet the computing time is between two and three times less. This remark attests to the efficiency of the FE-DVR method.

APPENDIX B: THE ROUNDOFF ERRORS IN THE FE-DVR METHOD

The notation is as follows: N is the number of Lobatto points in each partition, which is also equal to the number of Lagrange polynomials in each partition, and N_p is the number of partitions. The largest contribution to the roundoff errors is expected to arise from the solution of Eq. (23) for the $N-2$ expansion coefficients. This equation is of the type $\bar{M}\beta = b$, where β is the column vector of the $N-2$ expansion

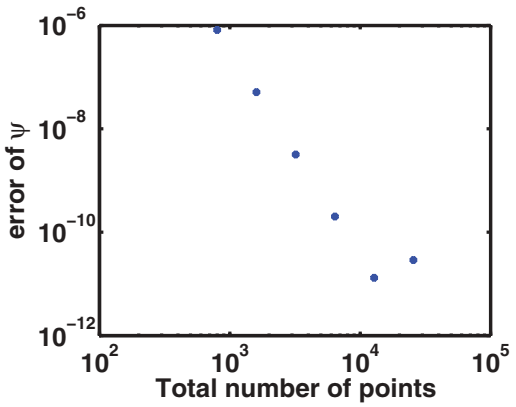

FIG. 12. (Color online) The error of the Numerov wave function at $r = 18$ fm as a function of the number N of mesh points in the interval [0,20 fm]. The distance h between points is $20/N$. For each h, the wave function is normalized to the S-IEM wave function at $r = 2$ fm. The wave number is $k = 0.5$ fm^{-1} and the potential is V_M.

coefficients and $\bar{M}$ is a matrix of dimension $N-2$, whose solution requires $4 \times (N-2)^3$ floating point operations. For the case in which the floating point roundoff error of the computer is ε and the errors accumulate linearly, an upper bound for the total error ε_T is

$$\varepsilon_T \approx 4N_P(N-2)^3\varepsilon. \tag{B1}$$

For $N_p = 100$ and $\varepsilon = 10^{-16}$, which is the value for the calculations done in MATLAB, one obtains an upper bound for the values of ε_T that are plotted in Fig. 6 as a function of N,

$$\varepsilon_T \approx 4 \times 10^{-14}(N-2)^3\varepsilon. \tag{B2}$$

The floating point error that occurs in the calculation of the Lagrange functions $\ell_i(x)$ is much smaller. The numerator contains N factors $x - x_i$, each of which can be written as $\Delta_i + \varepsilon$, where Δ_i is proportional to the length of each partition. Hence the error of the product is $\approx \Delta^N + N\Delta^{N-1}\varepsilon$, where Δ is an average value of $x - x_i$. A similar argument holds for the denominator, and if the error of the numerator adds linearly to the error of the denominator, then an upper bound for the total error of a Lagrange function is $\simeq 2N\varepsilon/\Delta$. This is much less than the error in Eq. (B1).

For the case of the nonlocal calculation, the conditions above are different. There is only one partition of length $L = 15$ fm, the number of Lobatto points is 130, and the order of each polynomial $\ell(r)$ is 129. The error in the calculation of the Lagrange polynomials, or their derivatives at each mesh point, is $\leqslant 2(N-1)\varepsilon/\Delta$. Since the error in the calculation of the matrix element of (d^2/dr^2) has N terms according to Eq. (5), that could lead to an error of $\simeq 2N(N-1)\varepsilon/\Delta$, assuming that all ε errors add linearly. The solution of Eq. (23) requires $4(N-2)^3$ operations, and thus an upper bound of the total linear accumulation of ε errors is

$$\simeq 2N(N-1)(\varepsilon/L)4(N-2)^3 = 1.8 \times 10^{-6}. \tag{B3}$$

TABLE III. The Numerov/FE-DVR ratio of the required total number of mesh points and the respective computational times.

Accuracy tan(δ)	Ratio of no. of points	Time ratio
10^{-6}	$\simeq 1$	20
10^{-8}	15	100

Since the ε errors do not accumulate linearly, the expected upper bound for the error could be

$$\leqslant 2(N-1)(\varepsilon/L)4(N-2)^3 = 1.4 \times 10^{-8}. \tag{B4}$$

The above estimate is consistent with the accuracy found numerically in Fig. 5.

APPENDIX C: COMPARISON WITH A FINITE-DIFFERENCE METHOD

The finite-difference method used for this comparison is Milne's corrector method, also referred to as the Numerov method, given by Eq. 25.5.21 in Ref. [23]. In this method, the error of the propagation of the wave function from two previous points to the next point is of order h^6, where h is the radial distance between the consecutive equispaced points. The calculation is done for the potential V_M and for $k = 0.5$ fm^{-1} as follows.

A value of h is selected and the Milne wave function is calculated starting at the two initial points $r = h$ and $2h$ by a power series expansion of the wave function for the potential V_M. The values of the wave function for the additional points $3h, 4h, \ldots$ are obtained from Milne's method out to the point $r = 20$ fm. The wave function is normalized to the S-IEM value at $r = 2$ fm, and the error at $r = 18$ fm is obtained by comparison with the S-IEM value at that point. The result for a sequence of h values is illustrated in Fig. 12. For each value of h, the wave function is calculated out to $r = 100$ fm by Numerov's method, and the integral (8) is calculated by the extended Simpson's rule, given by Eq. (25.4.6) in Ref. [23]. The error is determined by a comparison with the S-IEM result 2.699 470 250 2 for tan(δ). A comparison with the FE-DVR method is shown in Fig. 9, and Table III displays the ratio Numerov/FE-DVR of the total number of points and of the time of the two methods for two accuracies of tan(δ). More details of the error and the computing time for the Numerov method are displayed in Table IV.

The calculation is done in MATLAB performed on a desktop using an Intel TM2 Quad, with a CPU Q 9950, a frequency of 2.83 GHz, and a RAM of 8 GB.

TABLE IV. Accuracy and computing time for the Numerov method.

No. of points	Error [tan(δ)]	Time (s)
12 800	1.23×10^{-9}	51
6400	9.41×10^{-9}	5.8
3200	7.50×10^{-8}	2.1
1600	5.99×10^{-7}	1.0
800	4.76×10^{-6}	0.72

[1] D. O. Harris, G. G. Engerholm, and W. D. Gwinn, J. Chem. Phys. **43**, 1515 (1965); A. S. Dickinson and P. R. Certain, *ibid.* **49**, 4209 (1968).
[2] J. C. Light and T. Carrington Jr., Adv. Chem. Phys. **114**, 263 (2000).
[3] R. G. Littlejohn, M. Cargo, T. Carrington Jr., K. A. Mitchell, and B. Poirer, J. Chem. Phys. **116**, 8691 (2002).
[4] F. W. Olver, D. W. Lozier, R. F. Boisvert, and C. W. Clark, *NIST Handbook of Mathematical Functions* (National Institute of Standards and Technology, New York, 2010).
[5] K. J. Bathe and E. Wilson, *Numerical Methods in Finite Element Analysis* (Prentice Hall, Englewood Cliffs, NJ, 1976); O. C. Zienkiewicz, *The Finite Element Method: Its Basis and Fundamentals* (Elsevier, Oxford, 2005).
[6] J. Shertzer and J. Botero, Phys. Rev. A **49**, 3673 (1994).
[7] Z. Kopal, *Numerical Analysis* (Wiley, New York, 1961).
[8] V. I. Krylov, *Approximate Calculation of Integrals* (MacMillan, New York, 1962).
[9] D. E. Manolopoulos and R. E. Wyatt, Chem. Phys. Lett. **152**, 23 (1988).
[10] B. I. Schneider *et al.*, in *Quantum Dynamic Imaging: Theoretical and Numerical Methods*, edited by A. D. Bandrauk and M. Ivanov, CRM Methods in Mathematical Physics (Springer Science and Business Media, London, 2011), p. 149.
[11] H. Wei, J. Chem. Phys. **106**, 6885 (1997).
[12] M. J. Rayson, Phys. Rev. E **76**, 026704 (2007).
[13] B. I. Schneider and N. Nygaard, Phys. Rev. E **70**, 056706 (2004).
[14] T. N. Rescigno and C. W. McCurdy, Phys. Rev. A **62**, 032706 (2000).
[15] K. Balzer, S. Bauch, and M. Bonitz, Phys. Rev. A **81**, 022510 (2010).
[16] C. Y. Lin and Y. K. Ho, Phys. Rev. A **84**, 023407 (2011).
[17] S. X. Hu, L. A. Collins, and B. I. Schneider, Phys. Rev. A **80**, 023426 (2009).
[18] L. Tao, C. W. McCurdy, and T. N. Rescigno, Phys. Rev. A **79**, 012719 (2009); M. Hesse, J. M. Sparenberg, F. van Raemdonck, and D. Baye, Nucl. Phys. A **640**, 37 (1998); D. Baye, Phys. Stat. Sol. (b) **243**, 1095 (2006).
[19] A. T. Patera, J. Comput. Phys. **54**, 468 (1984).
[20] J. Tromp, D. Komatitsch, and Q. Liu, Commun. Comput. Phys. **3**, 1 (2008).
[21] L. N. Trefethen, *Spectral Methods in MATLAB* (SIAM, Philadelphia, PA, 2000); J. P. Boyd, *Chebyshev and Fourier Spectral Methods*, 2nd revised ed. (Dover, Mineola, NY, 2001); B. Fornberg, *A Practical Guide to Pseudospectral Methods,*Cambridge Monographs on Applied and Computational Mathematics (Cambridge University Press, Cambridge, UK, 1998).
[22] R. A. Gonzales, J. Eisert, I. Koltracht, M. Neumann, and G. Rawitscher, J. Comput. Phys. **134**, 134 (1997); R. A. Gonzales, S.-Y. Kang, I. Koltracht, and G. Rawitscher, *ibid.* **153**, 160 (1999); G. Rawitscher and I. Koltracht, Comput. Sci. Eng. **7**, 58 (2005); G. Rawitscher, *Applications of a Numerical Spectral Expansion Method to Problems in Physics: A Retrospective*, in Operator Theory, Advances and Applications, edited by T. Hempfling (Birkäuser Verlag, Basel, 2009), Vol. 203, pp. 409–426; A. Deloff, Ann. Phys. (NY) **322**, 1373 (2007).
[23] *Handbook of Mathematical Functions*, edited by M. Abramowitz and I. Stegun (Dover, New York, 1972).
[24] R. H. Landau, *Quantum Mechanics II* (Wiley, New York, 1990).
[25] F. G. Perey and B. Buck, Nucl. Phys. A **32**, 353 (1962).
[26] G. H. Rawitscher, Nucl. Phys. A **886**, 1 (2012).
[27] G. Rawitscher (submitted to Phys. Rev. A).
[28] G. Rawitscher and J. Liss, Am. J. Phys. **79**, 417 (2011).